

HIGH QUALITY InGaN FOR PHOTOVOLTAIC APPLICATIONS: TYPE AND SPATIAL DISTRIBUTION OF CRYSTALLINE DEFECTS AND “PHASE” SEPARATION

Nikolai Faleev¹, Balakrishnam Jampana², Anup Pancholi², Omkar Jani^{1,3}, Hongbo Yu³,
Ian Ferguson³, Valeria Stoleru³, Robert Opila², and Christiana Honsberg¹

¹Electrical and Computer Engineering, ²Material Science and Engineering, University of Delaware Newark, DE, USA

³School of Electrical and Computer Engineering, Georgia Institute of Technology, Atlanta, GA, USA

Corresponding author: jani@ece.gatech.edu

ABSTRACT

The III-nitride material system with band gap ranging from 0.7eV to 6.2eV has substantial potential to develop high-efficiency solar cells. The III-nitride materials are grown by MOCVD on a lattice mismatched sapphire substrate (0001). This paper presents the generation of extended crystalline defects and their spatial distribution in the GaN and $\text{In}_{0.12}\text{Ga}_{0.88}\text{N}$ layers as a function of $\text{In}_{0.12}\text{Ga}_{0.88}\text{N}$ thickness. The material is characterized by photoluminescence, and the primary peak intensity is observed to increase with thickness, up to 200 nm, but the intensity diminishes with further increase in thickness. Additional photoluminescence peaks are observed for $\text{In}_{0.12}\text{Ga}_{0.88}\text{N}$ thicknesses greater than 100 nm. These observations are attributed to extended crystalline defects and are characterized by high resolution x-ray diffraction. A detailed analysis of these extended crystalline defects is presented based on rocking curves, symmetric and asymmetric reciprocal space maps. The crystalline defects are unavoidable during epitaxial growth, but knowledge of their generation process yields better control over them.

INTRODUCTIONS

The III-nitride material system, which consists of aluminum nitride (AlN), gallium nitride (GaN), indium nitride (InN) and its alloys, offer substantial potential to develop high-efficiency solar cells. In addition to the direct wide-band gap range (0.7 – 6.2 eV), this material system is characterized by high theoretical mobilities, high absorption, high peak and saturation velocities [1], and radiation hardness. While the InGaN material system was identified as a potential photovoltaic material earlier [2], we have practically demonstrated record high V_{oc} 's for InGaN solar cells [3] and are in the process of further optimizing such devices [4].

One of the major challenges in the novel InGaN material system is based on material quality. First, due to the lack of availability of a suitable substrate in terms of lattice and thermal expansion coefficient mismatch, epitaxially grown InGaN measures a threading dislocation density in the $10^7 - 10^{10} \text{ cm}^{-2}$ range [5][6]. Secondly, there also exists a solid-phase miscibility gap in the InGaN alloy due to the large difference in lattice constant between InN and GaN [7][8]. Moreover, due to challenges associated with achieving thermodynamic equilibrium during epitaxy, non-stoichiometric growth conditions, and also stress arising from substrate mismatches, there is a tendency in InGaN to form lower-band gap instances during growth [9],

which is known as phase separation. Phase separation is identified as secondary peaks, or broadening of the primary InGaN peak in photoluminescence (PL) or x-ray diffraction (XRD) measurements.

Both, dislocations and phase separation have direct implications on the resultant solar cell performance. Both these types of defects act as recombination channels and lower the short-circuit current, as well as tend to pin the open-circuit voltage, thus lowering the overall efficiency of the resultant solar cell. Hence, it becomes critical to understand and control the process of defect formation during epitaxy in order to realize high-performance InGaN solar cells.

GROWTH AND CHARACTERIZATION

Epitaxial Growth

Thin undoped $\text{In}_{0.12}\text{Ga}_{0.88}\text{N}$ layers are grown on standard undoped-GaN/sapphire templates in an Emcore MOCVD reactor. Trimethylgallium (TMGa) and Trimethylindium (TMIn) are the precursors used to introduce gallium and indium, respectively, into the reactor using hydrogen as the carrier gas; while ammonia (NH_3) is used as the nitrogen source. The u-GaN layer is grown using a two step process, where typically a 20-40 nm thin GaN buffer layer growth at 550°C is followed by the epitaxy of high-quality 2 μm thick GaN template at 1030°C. Four $\text{In}_{0.12}\text{Ga}_{0.88}\text{N}$ Samples: A, B, C and D of respective thicknesses 50, 100, 200 and 400 nm, are grown on the template at 780°C. The growth rate of GaN is set at 2.15 $\mu\text{m/hr}$, while that of $\text{In}_{0.12}\text{Ga}_{0.88}\text{N}$ is 0.116 $\mu\text{m/hr}$.

Material characterization

Time-integrated PL measurements on the InGaN samples are conducted at 77K. The excitation source is a frequency doubled tunable Ti:Sapphire laser with an incident wavelength of 375 nm. High-resolution XRD studies are performed with an X'Pert diffractometer featuring Ge(220) four bounce monochromator, Ge(220) three bounce analyzer in triple-axis alignment with $\text{CuK}_{\alpha 1}$ monochromatic radiation. Reciprocal Space Maps (RSMs) of symmetrical (0002) and asymmetrical (11.4) reflections are collected.

RESULTS

PL and XRD for all investigated samples are

summarized in Tables 1-3, corresponding to GaN and InGaN layers. x-ray data for bare GaN layer is also added to Table 2. Simultaneous investigation of crystalline perfection of both GaN and InGaN epitaxial layers gives detailed information about crystalline perfection of entire epitaxial structure and allows correct interpretation of structural transformation of crystalline defects during epitaxial growth.

The structural data is interpreted by collectively analyzing two groups: more crystalline perfect samples, Samples A and B with the nominal thickness of InGaN layer 50 and 100 nm, and less crystalline perfect samples C and D with the nominal thickness of InGaN layers 200 and 400 nm.

Table 1. Photoluminescence Results

Sample	1 st Peak /FWHM (nm)	2 nd Peak / FWHM (nm)	Shoulder (nm)	In Composition (X-ray data)
A (50nm)	416.4 / 10.67	NA	NA	11.45
B (100nm)	422.05 / 7.44	437.2	451.8	12.45
C (200nm)	420.6 / 8.4	432.6 / 14.6 447.1 / 19.45	463.2 / 31.65	12.0
D (400nm)	416.3 / 12.4	431.05 / 16.96 448.3 / 17.2	467.2 / 18.7	11.6

Samples A and B

The PL peak intensity from InGaN increases with increasing thickness as seen from **Error! Reference source not found.** Measured PL peaks correspond to the band gap (~2.9eV) for 12% InGaN. The emergence of additional peaks at longer wavelengths is also evident for Sample B. The additional peaks can be correlated to the defects in the material and investigated by XRD.

Coherent ω -2 θ diffraction curves, Figure Fig. 2, measured in the vicinity of InGaN and GaN (0002) reflections have strong diffraction peaks, corresponding to the epitaxial layers and additional extended interference pattern around InGaN diffraction peak. Coherence length in both InGaN samples, A and B, is close to their layer thicknesses of 43 and 92 nm, respectively; non-homogeneity of the thickness, evaluated from the angle extent of the interference patterns is about 3.0 and 5.0 nm, respectively. This deterioration is caused by extended crystalline defects such as Dislocation Loops (DLs) or Stacking Faults (SFs), already created in the volume of the epitaxial layer; but it is not related to misfit or threading screw dislocations, which typically do not deteriorate vertical coherence of the scattering layer [10]. Indium composition is measured to be around 12% in all

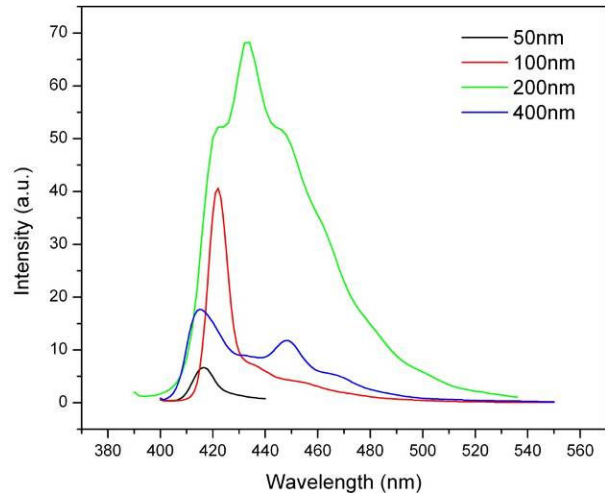


Fig. 1. Photoluminescence Results

samples as seen in Figure Fig. 2.

The density of threading screw dislocations is nearly the same in both samples A and B, and in both GaN and InGaN epitaxial layers, as analyzed from Figure 3. Such coincidence demonstrates that in spite of different growth conditions, the level of structural deteriorations during growth processes is nearly identical. These dislocations are so-called “primary threading dislocations”, which originate at the initial stage of the growth process near the GaN/sapphire-substrate interface to compensate the excess of point defects created at this moment. Under rather perfect growth conditions, these dislocations extend to the growth surface without noticeable change in density during the entire growth process.

In GaN epitaxial layers there is a clear trend to the diminution of the vertical coherent length from the reference GaN layer (i.e. without InGaN grown on top) to the GaN layer in Sample B, which is related with epitaxial growth of InGaN layer. This diminution is caused by spatial displacement of transformation sub-layer, already existing in a thick GaN layer, closer to the GaN/InGaN interface. This process of diffusion and accumulation of point defects results in creation of a transformation sub-layer. These defects can diffuse from their point of origin, in the InGaN layer, through the GaN/InGaN interface. After that they continue their inward diffusion and accumulate in the GaN layer at a distance determined by the diffusion length of point defects in GaN (~ 0.6 – 0.75 μ m in rather perfect GaN layers). These defects structurally transform here to extended crystalline defects under the action of self-induced secondary elastic stress [10].

The penetration of point defects through the InGaN/GaN interface is possible if the extent of relaxation of initial elastic stress between InGaN and GaN layers is low and corresponding density of misfit dislocations on this interface is not enough to block inward diffusion of point defects through the interface [5]. RSM patterns, measured on (11.4) asymmetrical reflection (Figure 4), confirm the lack of relaxation between InGaN and GaN layers. Though the thicknesses of InGaN layers in Samples A and B

significantly exceed the so-called “critical thickness” (approximately by 8 and 16 times, respectively) the accommodation of elastic strain at the InGaN/GaN interface is negligible ($\Delta q_x = 0$) in both samples. Preferred crystalline defects in both InGaN layers are “primary” threading screw dislocations, propagated from the bottom GaN layer, plus “frozen” point defects, which diffuse inward at the moment of growth process completion.

Samples C and D

Crystalline perfection of Samples C and D is noticeably deteriorated compared to Samples A and B. Structural deteriorations in both GaN and InGaN layers are related to the epitaxial thickness of grown InGaN layer.

The PL of Samples C and D demonstrate additional peaks as seen in Figure **Error! Reference source not found.** The intensity of sample D is lower due to diminished crystalline perfection. In GaN layers, the vertical coherent length significantly diminishes and stabilizes at 470 nm (Table 2). The density of threading screw dislocations increases approximately by two times, as analyzed from Figure 3. Entire erosion of interference pattern around InGaN peak in the ω - 2θ rocking curves (RCs), Figure Fig. 2c, shows the creation of transformation sub-layer in the volume of these layers. Vertical coherent length in InGaN layers significantly diminishes in comparison with the entire layer thickness; confirming creation of a transformation sub-layer. The density of threading screw dislocations in these layers increase significantly (3 – 10 times). On the other hand, angle position of InGaN peak remains immutable suggesting negligible relaxation of elastic stress at the GaN/InGaN interface. Asymmetrical RSM patterns reveal the initial stage of relaxation of elastic stress in both samples. While Δq_x in Sample D is 1.5 times more in comparison with C (Figure 4), it is still significantly less than expected for samples with complete relaxation.

DISCUSSIONS

At the initial stage of InGaN epitaxial growth, up to a thickness of 100 nm, the process of diffusion, accumulation and structural transformation of point defects iterates creating a transformation sub-layer in the GaN layer. Further continuation of growth and consequent increase in layer thickness significantly changes this situation. The critical point for these processes is the InGaN layer thickness, i.e. when the thickness of the growing layer becomes comparable with the diffusion length of point defects in this material. Before this critical point, most diffused point defects continue to penetrate into the GaN layer and transform to extended crystalline defects in there. As a result, this

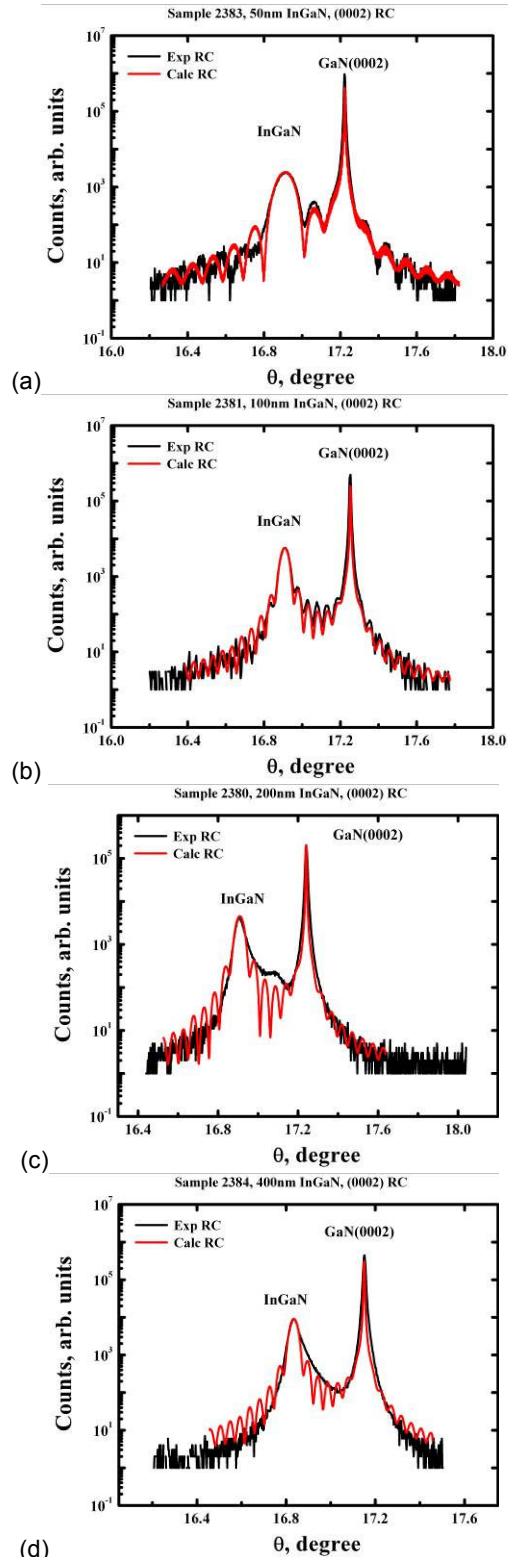


Fig. 2. ω - 2θ coherent RC, measured in the vicinity of Refl(0002), Experimental (blue) and Calculated (red) RCs (a) 50nm, (b) 100nm, (c) 200nm, and (d) 400nm

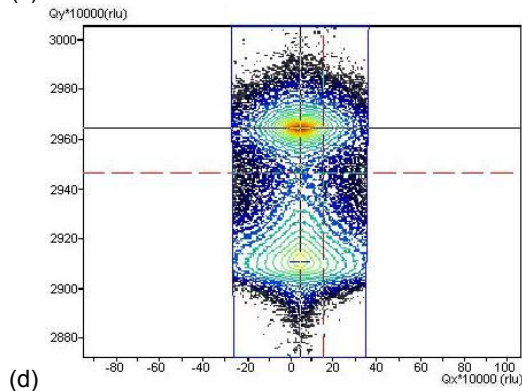
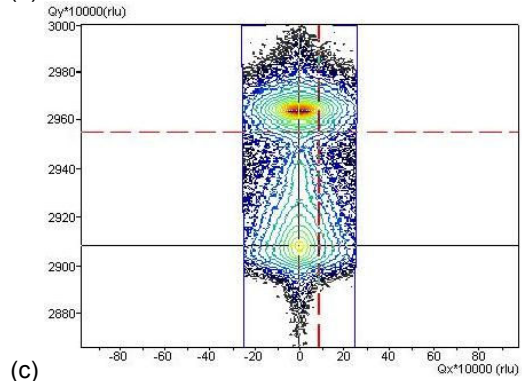
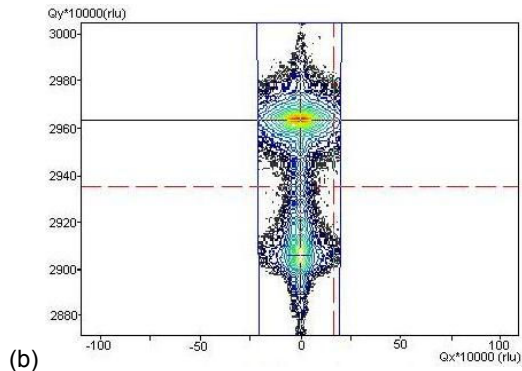
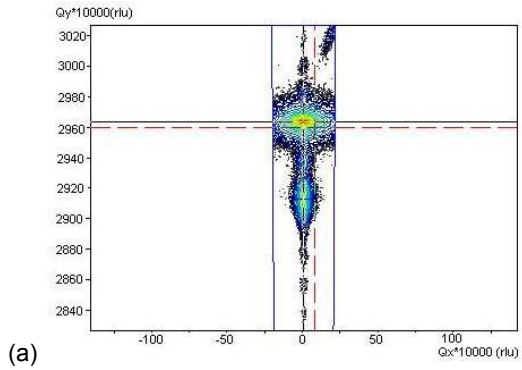


Fig. 3. Refl(0002), triple crystal symmetric reciprocal space map (a) 50nm, (b) 100nm, (c) 200nm, and (d) 400nm.

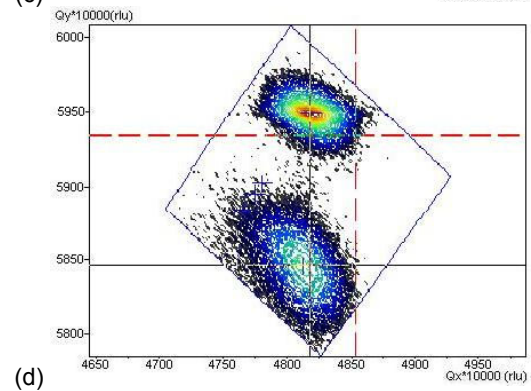
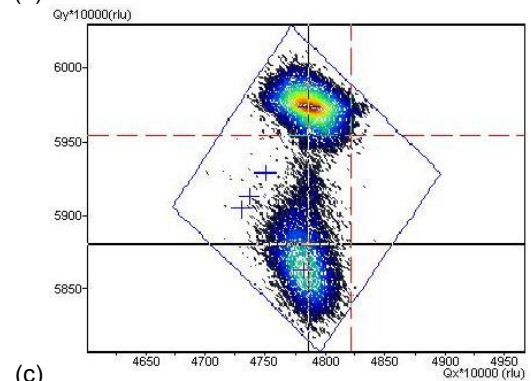
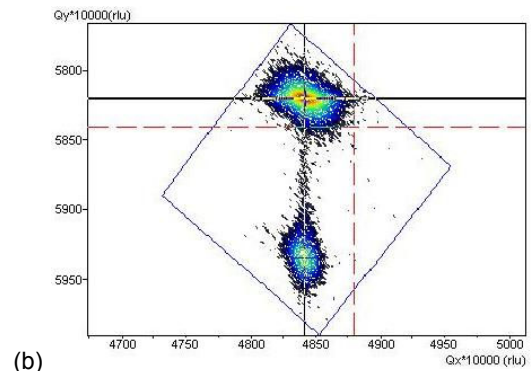
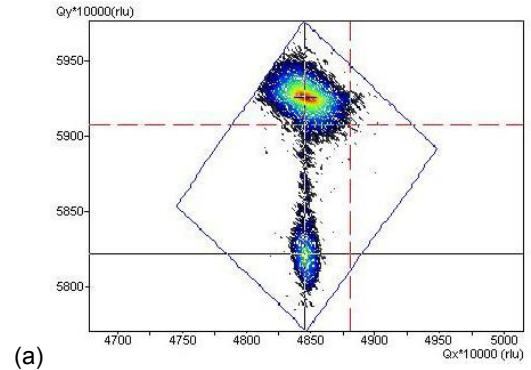


Fig. 4. Refl(0002), triple crystal asymmetric reciprocal space map (a) 50nm, (b) 100nm, (c) 200nm, and (d) 400nm.

Table 2. Parameters of GaN layers, x-ray (0002) RCs

Sample	ω -2 θ RC FWHM (arc.sec)	D _{Coher ⊥} (nm)	ω RC FWHM (arc.sec)	D _{Coher ∥} (nm)	N _{Thr. Disl} (cm ⁻²)
GaN Buffer Layer	21.2	785	315	168	3.4 x 10 ⁸
A (50nm)	22.7	733	290	184	2.8 x 10 ⁸
B (100nm)	25	670	300	178	3.0 x 10 ⁸
C (200nm)	35.3	470	425	125	6.0 x 10 ⁸
D (400nm)	35.3	470	400	135	5.3 x 10 ⁸

Table 3. Parameters of InGaN layers, x-ray (0002) RCs

Sample	ω -2 θ RC FWHM (arc.sec)	D _{Coher ⊥} (nm)	ω RC FWHM (arc.sec)	D _{Coher ∥} (nm)	N _{Thr. Disl} (cm ⁻²)	X _{In} (%)
A (50nm)	340	43	295	180	2.9 x 10 ⁸	11.45
B (100nm)	165	92	297	180	3.0 x 10 ⁸	12.45
C (200nm)	164	100	505/890	105/65	8.5 x 10 ⁸	12.0
D (400nm)	145	115	670/1070	80/50	1.5 x 10 ⁹ (3.6 x 10 ⁹)	11.6

transformation sub-layer shifts upward closer to the GaN/InGaN interface, and the density of threading dislocations increases due to creation of secondary threading dislocations.

Significant diminution of the coherent length (Table 2 and Table 3) and increase of the density of threading dislocations in comparison with the previous samples, A and B, and coincidence of these values in both Samples C and D shows that relaxation is initiated between InGaN thickness of 100 and 200 nm, and speculated to be closer to 100 nm. At greater thicknesses, the majority of created point defects begin to accumulate and structurally transform in the InGaN layer. Accumulation of point defects starts in the bottom part of the layers close to the GaN/InGaN interface. This process is accompanied by noticeable increase of secondary elastic stress in the layer. A combination of abundant point defects in the vicinity of the interface with an additional elastic stress triggers the partial accommodation of "initial" elastic strain and creation of "secondary" misfit dislocations at this interface. Due to a low growth rate, this situation is retained for a while; then the maximum of point defects and secondary elastic stress, following to the growth surface, shifts upward and the process of structural transformation of point defects and relaxation of secondary elastic stress continues in the volume of InGaN layer. This results in creation of extended crystalline defects in the volume of the layers, followed by their transformation to the secondary threading dislocations. In the thicker InGaN layer (Sample D) these processes continue for longer times and lead to higher density of secondary crystalline defects. As a result of these processes the structure of crystalline defects in Samples C and D is more complicated in comparison with Samples A and D.

In Samples C and D primary threading dislocations and "frozen" point defects are the main crystalline defects

at the top part of InGaN layers (100 – 115 nm). Below there is a transformation sub-layer with extended crystalline defects such as stacking faults or dislocation loops plus edge segments of threading dislocations (the type of defects can be verified by TEM, not studied in present work). It is hard to estimate the thickness of this sub-layer, but it is solid and thick enough to fully eliminate interference patterns on x-ray RCs. Deeper in the layer exist "secondary" threading dislocations, created below the transformation sub-layer due to dissociation of small extended defects. In Sample D, this area is thicker than that in Sample C. The density of misfit dislocations at the interface is higher due to the longer time available for structural transformation of accumulated point defects. In GaN, the transformation sub-layer is closer to the GaN/InGaN interface. The main crystalline defects at the top part of GaN layers (less than 470 nm) are "primary" threading dislocations and "frozen" point defects, which are diffusing from the top InGaN layer.

CONCLUSIONS

Correlation of PL and XRD allows better understanding of the main features of PL spectra. It reveals that threading screw dislocations and "frozen" point defects do not affect the shape and intensity of PL signal (Samples A and B). Increase of the intensity of the main peak in the spectrum of Sample B is related to the layer thickness, whereas a small shift of the peak position is determined by variation of indium composition in InGaN. Small additional peaks at higher wavelengths are caused by incipient clusters of point defects created at the bottom part of this layer. Further increase of the PL signal at the Sample C correlates with increased thickness of InGaN layer. Two additional strong PL peaks at longer wavelengths for Samples C and D are related to two different types of

extended crystalline defects, already created at the bottom part of this layer in the transformation sub-layer. Coincidence of the PL peak positions in Samples C and D means they are related to the same type of crystalline defects, stacking faults and edge segments of threading dislocations (the type can only be verified by TEM). The change in ratio of their intensity most probably correlates with the change of their density in these structures. Strong diminution of the total intensity of PL spectra for the Sample D is possibly related with non-radiative recombination in a more dense net of misfit dislocations, located on GaN-InGaN interface.

While crystalline defects are unavoidable in lattice mismatched epitaxial structures, they can be control by optimizing the growth conditions. Knowledge of growth conditions allows prediction of type and spatial distribution of crystalline defects and can lead to reliably engineered epitaxial material for high band gap solar cells.

REFERENCES

- [1] Y. Nanishi, Y. Saito and T. Yamaguchi, "R-F Molecular Beam Epitaxy Growth and Properties of InN and Related Alloys", *Jpn. J. Appl. Phys.*, **42**, 5A, 2003, pp. 2549-2559.
- [2] J. Wu et al, "Superior radiation resistance of In_{1-x}Ga_xN alloys: Full-solar-spectrum photovoltaic material system," *J. Appl. Phys.*, **94**, 2003, pp. 6477.
- [3] O. Jani, I. Ferguson, C. Honsberg, S. Kurtz, "Design and characterization of GaN/InGaN solar cells," *Appl. Phys. Lett.*, **91**, 2007, pp. 132117.
- [4] O. Jani, B. Jampana, M. Mehta, H. Yu, I. Ferguson, R. Opila, C. Honsberg, "Optimization of GaN window layer for InGaN solar cells using polarization effect," *Thirty third IEEE PVSC*, 2008 (To be published).
- [5] N. Faleev, C. Honsberg, O. Jani, I. Ferguson, "Crystalline perfection of GaN and AlN epitaxial layers and the main features of structural transformation of crystalline defects," *J. Crystal Growth*, **300**, 2007, pp. 246.
- [6] N. Faleev, H. Lu, W.J. Schaff, "Low density of threading dislocations in AlN grown on sapphire," *J. Appl. Phys.*, **101**, 2007, pp. 093516.
- [7] I. Ho, and G. B. Stringfellow, "Solid phase immiscibility in GaInN," *Appl. Phys. Lett.*, **69**, 1996, pp. 2701.
- [8] S. Chichibu, T. Azuhata, T. Sota, and S. Nakamura, "Luminescence from localized states in InGaN epilayers," *Appl. Phys. Lett.*, **70**, 2007, pp. 2822.
- [9] V. A. Elyukhin, S. A. Nikishin, "Internal Strain Energy of A_x³B_{1-x}³N ternary solid solutions of cubic modification," *Semicond. Sci. Technol.*, **11**, 1996, pp. 917.
- [10] N. Faleev, H. Temkin, I. Ahmad, M. Holtz and Yu. Melnik, "Depth dependence of defect density and stress in GaN grown on SiC", *J. Appl. Phys.*, **98**, 2005, pp. 123508.